JCTC Journal of Chemical Theory and Computation

Article

pubs.acs.org/JCTC

Analysis of Optical Activity in Terms of Bonds and Lone-Pairs: The Exceptionally Large Optical Rotation of Norbornenone

Barry Moore, II,[†] Monika Srebro,[†,‡] and Jochen Autschbach*[,†]

[†]Department of Chemistry, University at Buffalo, State University of New York, Buffalo, New York 14260-3000, United States

[‡]Department of Theoretical Chemistry, Faculty of Chemistry, Jagiellonian University, R. Ingardena 3, 30-060 Krakow, Poland

Supporting Information

ABSTRACT: Norbornenone, which has both a C═O and a C═C chromophore in a rigid bicyclic hydrocarbon framework, exhibits optical rotation (OR) an order of magnitude larger than that of similar molecules with only one of these chromophores (e.g., α-pinene). Its OR is also very sensitive to approximations in electronic structure calculations. The present study demonstrates a novel approach to interpret optical rotation using familiar concepts of chemical bonding, aided by first-principles calculations. A theoretical procedure is developed for analyzing the OR tensor components of a molecule in terms of individual bonds and lone pairs. The link between the chemist's bond and quantum mechanics is provided by localized molecular orbitals obtained from density functional theory (DFT) calculations. Delocalization of π orbitals is shown to play a crucial role in the large OR of norbornenone, as hinted by the DFT delocalization error inherent in many standard functionals and confirmed by detailed analysis. The OR contributions generated by the double bond in α-pinene are even stronger than that of norbornenone. The isotropic average, observed in solution or in gas phase, is small as a result of cancellation of tensor components with opposite signs. The electronic coupling and delocalization of the C═C π bond and the C═O oxygen π lone pair in norbornenone selectively enhance one of the OR tensor components, resulting in the exceptionally large negative isotropic OR.

1. INTRODUCTION

Natural optical activity, such as optical rotation (OR) and circular dichroism (CD) caused by collections of randomly oriented chiral molecules interacting with UV−vis frequency electromagnetic waves, is of fundamental interest in the physical sciences and of great practical importance in organic and natural products chemistry as well as in other chemical disciplines. OR is one of the physical effects that can distinguish between the enantiomers of a chiral molecule. Yet, it is fair to state that OR is a poorly understood phenomenon in the sense that its sign and magnitude for a particular molecule are difficult to predict without performing an accurate ab initio calculation. Even with calculations at hand, it is very difficult to rationalize the results. "What is needed is the ... work of spectroscopists, quantum mechanicans, and theoretical chemists and physicists."[1]

Tremendous progress has taken place since 1962, when Tinoco made the above statement more generally about optical activity. Among the semiempirical theoretical methods that have provided highly valuable insight into the mechanisms of electronic optical activity (CD and/or OR), we mention the Applequist atom−dipole interaction model,[2] models based on coupled chromophores or coupled atom groups,[3−7] and the electron-on-a-helix.[8] Over the past 15 years, the development of ab initio methods for computations of optical activity has made huge strides, and their practical value has been clearly demonstrated.[9−15] Chemists are now in a position to tackle century-old questions about optical activity with the help of first-principles theory. However, an intuitive understanding of how structure and bonding relates to the sign and the magnitude of the OR for a molecule is still lacking. In 1998, Kondru, Wipf, and Beratan made a first attempt at dissecting isotropic ORs calculated at the Hartree−Fock (HF) level into atomic contributions with the help of a Mulliken-type partitioning.[16,17] Recently, Murphy and Kahr pointed out that nonchiral planar polyaromatic hydrocarbons (PAHs) have larger OR tensor elements than their chiral counterparts, the [n]-helicenes.[18] For helicenes the isotropic average does not vanish, whereas for nonchiral PAHs it does. The work highlights the tensorial nature of OR.[19] The present study intends to provide a first new step toward tackling the old problem of rationalizing OR with the help of molecular orbital (MO) analyses of optical rotation tensor elements.

The OR of norbornenone (Figure 1) has for a long time been of interest,[20] to both theoreticians and experimentalists. Norbornenone has an exceptionally large isotropic OR ($[\alpha]_D$= -1.1×10^3 deg/[dm (g/cm^{-3})], $[\phi]_D$= -1.2×10^3 deg cm^2/dmol in hexane[21]) compared to related molecules, for example norbornanone and α-pinene, with either a C═O or a C═C chromophore; both these molecules have specific rotations not exceeding about ±50 deg/[dm (g/cm^{-3})] in magnitude[22,23] (see Figure 1). It has been speculated long ago that the OR of norbornenone is exceptionally large because of an electronic interaction between the two chromophores.[20] Another reason for the interest in norbornenone is that its OR is very sensitive to approximations in electronic structure calculations. The B3LYP/aug-cc-pVDZ OR for norbornenone is almost identical to the experimental solution-phase value.[24,25] However, at the coupled cluster (CCSD) level of theory the OR drops to about half this experimental value.[26−29] The OR magnitude from Hartree−Fock (HF) calculations is somewhat lower than

Received: September 27, 2012
Published: September 28, 2012

   dx.doi.org/10.1021/ct300839y | J. Chem. Theory Comput. 2012, 8, 4336−4346

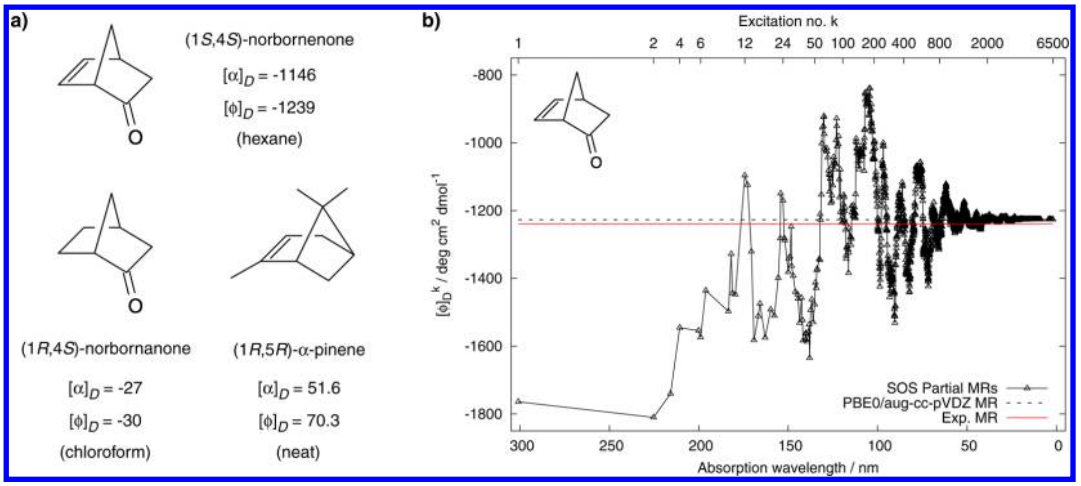

Figure 1. (a) Some bicyclic organic molecules and measured specific and molar optical rotations (in usual units) for λ = 589.3 nm. (b) SOS molar optical rotation of norbornenone (PBE0/aug-cc-pVDZ). Experimental solution-phase OR and the result from a direct calculation of the OR are indicated by horizontal lines. Note the slow convergence of the SOS.

CCSD but similar, which may hide the important role of correlation.[30] A strong reduction relative to B3LYP, albeit less drastic than with CCSD or HF, is also obtained with hybrid density functionals with range-separated exchange[30,31] and with the approximate coupled-cluster CC2 method.[27,29]

Attempts to rationalize the OR of norbornenone and other molecules based on the 'sum−over−states' (SOS) expression for OR found that the SOS analysis is of limited value.[25] See also refs 32−34 for related discussions. In the transparent region where the light-wave (circular) frequency ω is well below any of the electronic excitation frequencies, the SOS molar rotation (MR) is given by

$$[\phi]_\omega = 91.4303\omega^2 \sum_{j\neq 0} \frac{R_j}{\omega_j^2 - \omega^2}$$

Here, the R_j are the rotatory strengths for the electronic excitations in cgs units of 10^{-40} esu^2 cm^2, the ω_j are the excitation frequencies, and the numerical conversion factor gives the molar rotation $[\phi]$ in deg cm^2/dmol. For norbornenone, a dominant influence from the HOMO−LUMO transition, with the HOMO involving both π systems, was demonstrated in ref 25. A calculation of the SOS optical rotation of norbornenone with the PBE0 hybrid functional performed in our laboratory demonstrates the aforementioned behavior, as shown in Figure 1. However, the optical rotation oscillates hundreds of degrees as more excitations are included in the SOS. The slow convergence toward a result from a linear-response (LR) OR calculation, equivalent to a full SOS without explicit calculation of excited states,[35] is evident. It is noted that, because of the limited atomic orbital (AO) basis set, most of the calculated excited states are unphysical, but they are needed as a basis set to fully converge the SOS. For other molecules there is often not even a dominant term from a low-energy transition. Even in such a fortunate case as norbornenone, SOS expansions tend to be difficult to interpret.

As a first example of rationalizing OR, computed from first principles, in terms of chemist's bonds and lone pairs, the present work is devoted to a detailed analysis of the OR of norbornenone, focusing on several aspects: (i) It is shown that the large magnitude and sensitivity of the norbornenone OR can be traced back to one of the principal components of the OR tensor for which the field direction is roughly parallel to the C═O bond. (ii) We present a breakdown of this critical OR tensor component in terms of contributions from individual canonical and localized molecular orbitals, which represent bonds and lone pairs in quantum chemical calculations, and their perturbations by electric and magnetic fields. The role of the delocalization of the C═O and C═C chromophores becomes readily apparent from the analysis. (iii) The exceptional sensitivity of the OR for norbornenone to approximations in the electronic structure is investigated in the context of density functional theory (DFT). Herein, we focus in particular on the DFT delocalization error, which is shown to influence the coupling between the C═O and C═C chromophores, providing important clues about the large magnitude of the norbornenone OR. An 'optimally tuned' functional with range-separated exchange ensures a very small DFT delocalization error. The performance of this functional in terms of the OR is comparable to CC2. (iv) A physically motivated analysis protocol for the OR tensor components is proposed, by which the molecule is oriented such that the tensor representing the observable orientation-dependent optical rotation is diagonal in the laboratory coordinate frame.

Section 2 summarizes the theory and the analysis protocol for optical rotation used in this work. Section 3 provides computational details. Section 4 presents the results and discussion, including an investigation of the sensitivity of the norbornenone optical activity to the DFT delocalization error, a two-dimensional tuning of a fully long-range corrected hybrid functional to minimize said error, and a detailed analysis of the OR in terms of molecular orbital contributions including a comparison with α-pinene. Concluding remarks are provided in Section 5.

2. ANALYSIS PROTOCOL FOR ELECTRONIC OPTICAL ACTIVITY

The Supporting Information (SI) and ref 36 provide most of the theory underlying the adopted analysis protocol. A synopsis follows: The OR parameter β is a function of frequency ω (or, alternatively, wavenumber $\tilde{\nu} = \omega/(2\pi c)$ or wavelength $\lambda = 1/\tilde{\nu}$), and it is the molecular parameter that dictates the observed isotropic optical rotation. The OR parameter can be converted to a molar optical rotation in deg cm^2/dmol via

$$[\phi]_{\tilde{\nu}} = 1.3423 \times 10^{-6}\tilde{\nu}^2\beta(\tilde{\nu})$$

where β is in atomic units (au). The specific rotation $[\alpha]$ in units of deg/[dm (g/cm^{-3})] is obtained from the numerical value of $[\phi]$ multiplied by $100/M$, where M is the molar mass of the chiral molecule in g/mol. For additional details, see refs 11 and 37.

The (isotropic) OR parameter is the average $\beta = (1/3)\sum_u \beta_{uu}$ of a rank-2 OR tensor $\boldsymbol{\beta}$ with components β_{uv} referring here to the Cartesian laboratory frame. Typically, the diagonal elements of the OR tensor are much larger than the isotropic average and have positive and negative signs (see ref 36 for an example). A large isotropic OR is therefore often created not only by the OR tensor elements being large in magnitude but also by a strong imbalance in the magnitudes of the positive and negative components. A full understanding of the OR of a chiral molecule must therefore consider individual elements of the OR tensor. Another aspect is the behavior of $\beta(\omega)$ as a function of frequency. As ω approaches an electronic excitation frequency, the OR parameter (and the tensor elements) may strongly increase in magnitude (optical rotatory dispersion, ORD, see the denominator in the SOS expression), and go into a so-called anomalous dispersion regime as ω passes through an excitation. 'Intrinsic' reasons for why an OR is large or not may therefore overlay with the OR dispersion. For this reason, we suggest that both the static limit of β ($\omega = 0$) and its dynamic counterpart (nonzero ω) should be considered.

It is important to note that while in exact theory β is independent from the chosen coordinate origin, as an observable physical quantity must be, the elements of the tensor $\boldsymbol{\beta}$ are not (not even the diagonal elements β_{uuu}). Further, an element β_{uu} enters the equation of the observed orientation-dependent optical rotation for nonisotropic samples in the two directions perpendicular to u. For instance, β_{zz} contributes to the observable optical rotation in directions x and y for a fixed molecular frame. Refs 36, 38, 39, and the SI, for instance, provide an expression for a tensor $\tilde{\mathbb{B}}$, which has origin-independent elements $\tilde{B}_{uv}$ and for which the optical rotation parameter measured in the direction of a normalized directional vector $\boldsymbol{n}$ (defined in the laboratory coordinate system) is given by $\beta_n = \boldsymbol{n}\cdot\tilde{\mathbb{B}}\boldsymbol{n}$. Further, the tensors $\tilde{\mathbb{B}}$ and $\boldsymbol{\beta}$ have the same isotropic average (= β), which is obtained from averaging β_n over all possible orientations of $\boldsymbol{n}$.

We refer to $\tilde{\mathbb{B}}$ as the 'chiroptical response tensor' because it provides the observable orientation-dependent optical rotation in response to applied dynamic electric and magnetic fields. It is therefore physically meaningful to adopt a molecular orientation with respect to the laboratory coordinate system where $\tilde{\mathbb{B}}$ is diagonal (principal axis system, PAS). One can then separately analyze the three principal components of $\tilde{\mathbb{B}}$ and its constituents, in particular, the diagonal elements of $\boldsymbol{\beta}$, in the same coordinate frame.

A detailed understanding of the origin of the natural isotropic optical activity of a chiral molecule may be derived from a chemically motivated decomposition of the elements of $\boldsymbol{\beta}$. In a molecular-orbital (MO) based computational scheme such as Kohn–Sham (KS) time-dependent DFT (TDDFT), the isotropic optical rotation can be quantified as[36]

$$\beta(\omega) = -\frac{2}{3}\mathrm{Im}\sum_{u=x,y,z}\sum_i \left\langle \frac{\partial\varphi_i}{\partial E_u(+\omega)} + \frac{\partial\varphi_i}{\partial E_u(-\omega)} \middle| \frac{\partial\varphi_i}{\partial B_u(0)} \right\rangle := \frac{1}{3}\sum_{u=x,y,z}\sum_i \int \beta^i_{uu}(\mathbf{r})\,\mathrm{d}V \quad (1)$$

In the equation, φ_i is a molecular orbital with occupations of 2, E_u and B_u are components of a perturbing electric and magnetic field, respectively, in the u-direction. The right-hand side introduces a short-hand notation $\beta^i_{uu}(\mathbf{r})$ used in Section 4.3 to refer to the real functions of 3D space that are being integrated to obtain each term. The function $\beta^i_{uu}(\mathbf{r})$ may be thought of as an OR tensor component 'density' for a given orbital, which can be easily visualized. Equations to obtain the orbital derivatives are solved at zero field-strength for an electric field with frequency ω (corresponding to the light frequency for which the OR parameter is calculated) and a static magnetic field. It is important to note that eq 1 is exact in exact KS TDDFT. In practice, approximations such as finite basis sets and approximate density functionals are employed in order to make the first-principles computations feasible.

In essence, per eq 1, the optical rotation tensor element β_{uu} is made up from a sum of the overlaps of an electric-field perturbation and a magnetic-field perturbation for each MO. A Hartree–Fock analog for the static limit ($\omega = 0$) of β has been derived by Amos, in 1982.[40] The general version for TDDFT and for $\beta(\omega \neq 0)$ has been derived recently by one of us.[36] For the analysis, the φ_i in eq 1 can be the usual (canonical) MOs (CMOs), which are convenient to adopt if one wants to interpret the optical rotation in terms of electronic excitations. However, one may also employ a set of localized MOs (LMOs) that represent individual bond, lone-pair, and core orbitals to develop an understanding of the optical activity of a molecule based on these 'chemistry textbook orbitals' and eq 1 directly. The analysis protocol adopted here is summarized in a flowchart (Figure 2).

3. COMPUTATIONAL DETAILS

Optimized B3LYP/6-311G(d,p) geometries of norbornenone and α-pinene were taken from ref 31 in the (S, S) absolute configurations (compare Figure 1). All calculations were performed with a locally modified version of the Northwest

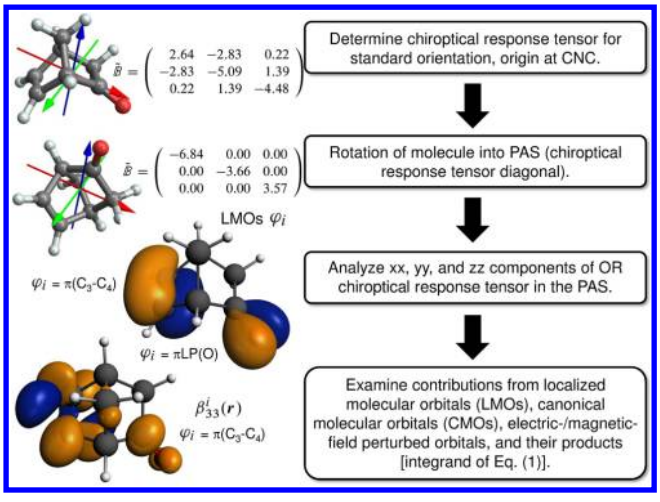

Figure 2. Flowchart for OR analysis. CNC = center of nuclear charges, PAS = principal axis system of $\tilde{\mathbb{B}}$.

Computational Chemistry (*NWChem*)[41,42] software package. The 'two-dimensional' tuning of the parameters α and γ in the range-separated exchange kernel of a fully long-range corrected (LC, $\alpha + \beta = 1$, see the SI for definitions of the parameters) hybrid variant of the Perdew–Burke–Ernzerhof exchange-correlation (XC) functional[43−45] was performed for norbornenone using the procedure from ref 46. LC refers to the fact that this functional affords the correct asymptotic behavior of the potential, unlike 'pure' (nonhybrid) or global-hybrid functionals (unless they are shape-corrected). The tuning employed a triple-ζ valence polarized (TZVP) Gaussian-type basis set[47] and was accomplished as outlined in the SI. To examine the dependency of the energy on the fractional electron number, $E(N)$, a series of single-point energy calculations for norbornenone, using fractional orbital occupations and fractional total electron numbers, was performed utilizing a code implemented previously by one of us.[30]

With the exception of the SOS data of Figure 1, all optical rotation (OR) and circular dichroism (CD) calculations were performed using the TDDFT linear response code as implemented in *NWChem*. See ref 36 for details. The excitation data used for the SOS were calculated with *Turbomole*, version 5.7.[48] In these calculations, the aug-cc-pVDZ basis set[49,50] (which includes diffuse functions needed for reasonably well converged optical response properties) was used. Equation 1 is valid for a complete basis set. To ensure that our finite-basis results give strictly origin invariant chiroptical response tensor elements, we have adopted a dynamic gauge-including atomic orbital (GIAO) basis set.[36,51] With GIAOs, there are additional terms in eq 1 that are included in the numerical analysis but omitted from the graphical representation of the magnetic-field perturbed orbitals in Section 4.3. Tables S1, S2, and S3 of the SI provide data showing that the analyses with, and without, GIAO contributions yield equivalent results and that the basis set used in this work is adequate for the task at hand. Some calculations applied the AO dipole length gauge as well as AO modified dipole velocity gauge, MVG,[52] and demonstrate very good agreement (see Table S1, SI). The optical rotation parameters were computed at the static limit $\lambda \rightarrow \infty$ nm ($\omega = 0$ au), the sodium D-line wavelength, 589.3 (0.07732), as well as $\lambda = 355$ ($\omega = 0.128$) and 633 nm (0.0720 au). The calculations involved both tuned as well as standard XC functionals such as PBE,[43] B3LYP,[53−55] and the conventional parametrization of LC-PBE0[56] along with HF. The localized orbitals generated for the LMO analysis of the OR were obtained with the Pipek–Mezey localization criterion.[57] We also used the *NBO 5.0* program[58] to generate localized orbitals and to analyze the extent of their delocalization. In Sections 4.3 and 4.4, numerical integrations of OR densities inside isosurfaces were carried out using isosurface values of 5×10^{-6} au (Figure 6) and 8×10^{-3} au (Figure 8). The software tools used to create the analysis data and cube files for the visualizations are available in the development version of the open-source quantum chemistry package *NWChem* and will be included in future releases. Isosurface plots of volume data were created with the graphical user interface of the Amsterdam Density Functional package (www.scm.com).

4. RESULTS AND DISCUSSION

We show in Sections 4.1 and 4.2 that the optical rotation of norbornenone is very sensitive to the extent of electron delocalization and that an optimally tuned functional (dubbed LC-PBE0*) ensures a physically reasonable delocalization. PBE and B3LYP give a much too delocalized electronic structure, while the bonds and lone pairs are too localized in HF theory. In Section 4.3, the delocalization of the C=C π bond and the C=O oxygen π lone pair is linked directly to the magnitude of one critical OR tensor component. The large isotropic OR is addressed in Section 4.4, by comparison with α-pinene. First, the sensitivity of the optical activity for norbornenone to the electronic structure is discussed because it provides important clues about the mechanisms at work.

4.1. General Assessment of the Calculations. Table 1 collects calculated vertical excitation energies, the associated rotatory strengths, and molar optical rotations for different wavelengths together with available experimental solution-phase data for norbornenone. The strong sensitivity of the OR for norbornenone to the choice of a density functional has been noted previously.[30,31,59] At the Na D-line ($\lambda = 589.3$ nm), the molar rotation increases by almost a factor of 3 in magnitude when going from HF theory to the pure functional PBE. The excellent agreement of B3LYP and PBE0 with the solution-phase OR at this wavelength[31] is likely a case of having the right results for the wrong reasons. Coupled-cluster (CC) data and recent gas-phase measurements of the OR for norbornenone[75] are significantly smaller in magnitude. We consider the CC data as accurate for the purpose of assessing different functionals. The results obtained with the stock parametrization of the LC-PBE0 functional and an optimally tuned version LC-PBE0* (Section 4.2), which afford the correct asymptotic behavior of the XC potential, are therefore superior to B3LYP and PBE0, and, obviously, PBE.

Table 1. First Electronic Vertical Excitation and Molar Rotation Values of Norbornenone Obtained with Different Computational Methods[a]

			$-[\phi]_\lambda$		
	E	$-R$	355	589.3	633
HF	4.90	45.0	3389	645.6	537.8
LC-PBE0	4.29	39.1	6345	893.0	735.3
LC-PBE0*[b]	4.36	44.5	6305	920.0	758.2
B3LYP	4.07	56.8	12371	1291	1051
PBE	3.74	69.3	39376	1932	1547
CC2[c]	4.26	37.6		1081/879.2	
			(6699)	(880.6)	(721.4)
CCSD[c]	4.30	23.1		800.9/602.9	
			(4213)	(605.5)	(498.3)
expt.[d]	4.02	51		1239	

[a]Energy E in eV. Rotatory strength R in 10^{-40} esu^2 cm^2. Molar rotation at specified wavelengths λ in nm, $[\phi]$, in deg cm^2/dmol. [b]Optimal parametrization as determined in this work. See Section 4.2. [c]Velocity aug-cc-pVDZ(C, O)+cc-pVDZ(H) E and R values from ref 26. Length (LG)/modified velocity gauge (MVG) aug-cc-pVDZ(C, O)+cc-pVDZ(H) $[\phi]$ results from refs 26−28. In parentheses, MVG aug-cc-pVDZ $[\phi]$ values from ref 29 are listed. [d]Solution phase. E and R values from ref 60. $[\phi]$ values from ref 21.

Based on the SOS molar rotation shown in Figure 1 and the discussion by Wiberg et al. in ref 25, the lowest electronic excitation has a strong influence on the OR at optical and near-UV wavelengths. The low magnitudes calculated with HF may therefore be associated, in part, with the particularly strong overestimation of the excitation energy. PBE at the opposite extreme has a much too low excitation energy, which translates to a vertical absorption wavelength of 331.5 nm rendering the

OR at 355 nm unreliable. Further, the PBE rotatory strength of the excitation is much too large in magnitude. LC-PBE0 and LC-PBE0* results are similar to CC2, both for the excitation data and for the molar rotations. When comparing the coupled-cluster results it is unclear, however, if the CC hierarchy is converged since CCSD corrects the CC2 molar rotations back toward the HF value. The data indicates that this happens mostly via a reduction of the rotatory strength of the lowest excitation. We note that there are large discrepancies between length and velocity gauge CC results, with the latter (see Table 1) being much lower in magnitude. The reported CCSD rotatory strength is also for the velocity gauge,[26] and therefore, its small magnitude may be related to basis set incompleteness, which appears to affect the CC data more strongly than the TDDFT results.

4.2. Role of Electron Delocalization. Electron correlation has, evidently, a major effect on the electronic optical activity of norbornenone, although it is somewhat hidden when CCSD and HF are compared. Available exchange-correlation density functionals afford an approximate treatment of electron correlation. However, the approximations also introduce deficiencies in the electronic structure that are not simply described by 'not enough correlation'. In the context of calculating refractive and absorptive properties such as OR and CD, the wrong asymptotic behavior of the XC potential for pure functionals and global hybrids (such as PBE and B3LYP) and the DFT delocalization error[61] are particularly noteworthy. The former deficiency is related to the known failure of TDDFT to predict charge-transfer excitations and excitations into diffuse states correctly. The latter is responsible for many shortcomings in DFT and TDDFT calculations, by causing the electronic structure to be too delocalized (typical for pure functionals) or too localized (typical for HF).[61,62] The two problems, to some degree, are interconnected.

The DFT delocalization error can be investigated via the behavior of the molecular energy (E) as a function of fractional electron number (N).[61,62] The correct behavior would display linear segments of E for N ranging between integers with slopes equal to the negative ionization potential of the species with nearest higher integer N. Figure 3 shows $E(N)$ of norbornenone for HF and selected density functionals. PBE and B3LYP exhibit pronounced positive curvature, which is indicative of too much delocalization. HF displays negative curvature, which is indicative of not enough delocalization (i.e., a too strong localization). LC-PBE0 by construction has the correct asymptotic behavior of the XC potential. It produces a comparatively small curvature of $E(N)$ for norbornenone. Its rather good performance in the optical activity calculations may be therefore attributed to the comparatively small DFT delocalization error, as well as to an accurate description of low-energy diffuse states, which are known to affect the optical activity of bicyclic molecules such as the ones shown in Figure 1. In terms of the SOS interpretation of the OR, one may think of the lowest-energy transition of norbornenone acquiring a too strong partial charge-transfer character with PBE and B3LYP (or PBE0), which causes significantly too low calculated excitation energies. It has recently been shown that seemingly unproblematic $\pi-\pi^*$ transitions in conjugated hydrocarbons may suffer from the same problem.[63]

Although the stock parametrization of LC-PBE0 is close to the desired behavior, it is not optimal. Can the functional be improved further? It is known that the exact functional affords $-\varepsilon^{\mathrm{HOMO}}(N) = \mathrm{IP}(N)$ for a system with N electrons, where

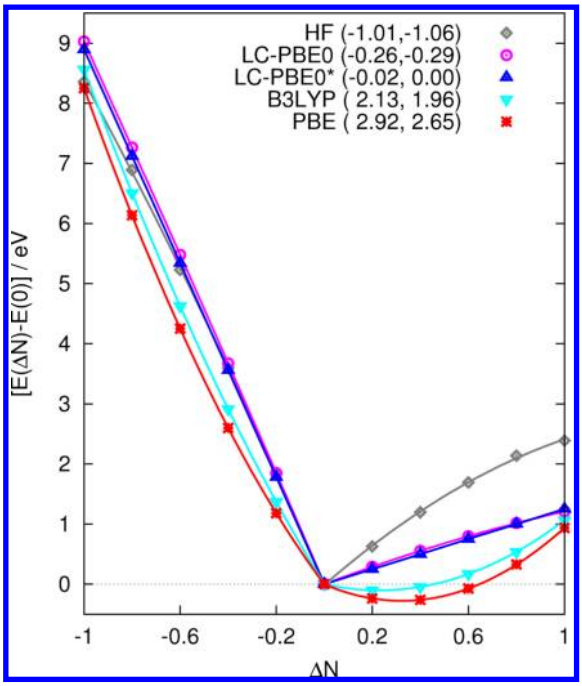

Figure 3. Energy of norbornenone as a function of fractional electron number, ΔN, relative to neutral system ($\Delta N = 0$). The numerical values in the plot key correspond to $(\Delta N)^2$ coefficients of quadratic fits to $E(N)$ in the electron-deficient and electron-rich regime, respectively ($\Delta N < 0$, $\Delta N > 0$), and therefore measure the curvature.

$\varepsilon^{\mathrm{HOMO}}$ is the energy of the highest occupied molecular orbital (HOMO).[64,65] If the functional is sufficiently flexible, this criterion can be satisfied for one or more species with different N, specifically for a given molecule, in order to improve the functional. The procedure has also been shown to give an excellent approximation of the fundamental gap, IP−EA, by the HOMO−LUMO gap.[66] Our group has recently investigated optimally tuned range-separated hybrid functionals[30,46,63,65,67,68,76] for the purpose of OR calculations,[30] but the approach was limited to tuning via the range-separation parameter in the expression for the inverse interelectronic distance in the range-separated exchange. Following more recent works,[46] we extend the approach here to consider all parameters in the range-separated exchange kernel of LC-PBE0, under the constraint that the potential affords the correct asymptotic behavior. This leaves two degrees of freedom, which is the reason we refer to the procedure as a two-dimensional functional tuning. Details are provided in the SI. Indeed, an optimal functional for norbornenone emerges that has the correct asymptotic behavior, meaningful frontier orbital energies, and an essentially vanishing DFT delocalization error (see Figure 3). We label this functional by LC-PBE0*. It needs to be emphasized that the tuning is not semiempirical but rooted in first-principles theory, based on known energetic criteria that a density functional should satisfy. Among other factors, its accuracy is constrained by the correlation that the PBE functional can provide.

Referring to the LC-PBE0* chiroptical data in Table 1, compared to the stock parametrization of LC-PBE0 the corresponding molar rotations calculated with LC-PBE0* are larger at long wavelengths, but not dramatically so. The calculated lowest excitation energy is slightly higher than those predicted by the LC-PBE0 functional and by CC theory, but still close. The performance appears to be comparable to CC2,

Table 2. Composition of Selected LMOs of Norbornenone in Terms of Weight from Atomic Hybrids at Different Centers[a]

	$\pi(C_1{=}O)$			$\pi(C_3{=}C_4)$				$\pi LP(O)$		
	O	C_1	$C_2 + C_6$	C_3	C_4	C_2	C_1	O	C_1	$C_2 + C_6$
HF	70.4	29.2	0.172	49.6	48.3	0.277	0.617	95.1	2.60	2.12
LC-PBE0	67.4	32.1	0.185	49.3	48.5	0.285	0.651	93.9	3.23	2.65
LC-PBE0*	67.9	31.6	0.189	49.3	48.4	0.297	0.712	94.0	3.18	2.60
B3LYP	67.1	32.4	0.207	49.1	48.3	0.315	0.804	93.4	3.42	2.83
PBE	66.1	33.3	0.222	48.9	48.2	0.329	0.903	92.6	3.81	3.12

[a]Numerical data obtained from 'natural LMOs' generated by the NBO program. All values in percent. Atom numbering as in Figure 5.

although a one-to-one comparison is difficult because of the different basis set requirements in DFT and CC theory to describe electron correlation.

Before turning to the OR analysis, it is important to establish a direct link between the DFT delocalization error indicated by the $E(N)$ curvature and the delocalization of the orbitals in the system. Since canonical MOs are delocalized by construction, we ask the question "How delocalized are the localized orbitals?" when calculated with different functionals (see ref 69 for further discussion). To obtain numerical data, we have employed the Natural Bond Orbital (NBO) procedure, devised by Weinhold et al.,[70] which provides a convenient breakdown of its 'natural' LMOs into contributions from different atoms. Note that the LMOs generated by the NBO program are very similar to those obtained from the Pipek−Mezey criterion, which are used for the numerical analysis of the OR in the next section. For graphical visualization of the latter, using different isosurface values, see Figure S2 in the SI. Table 2 provides selected examples that demonstrate the extent of electron delocalization and covalency in norbornenone (see also Table S5 in the SI). The π orbital of the C═O bond shows a clear trend of larger oxygen contribution when going from PBE to HF. More importantly, one oxygen lone pair in the C═O moiety, which is implicated in the OR by virtue of its participation in the lowest-energy transition in the SOS, shows a clear trend of being more delocalized over neighboring centers when going from HF theory to the pure functional PBE. Likewise, the C═C π orbital has a small contribution at the carbonyl carbon, which increases from HF to PBE. For comparison, the corresponding σ orbitals have an order of magnitude smaller contributions at distant atoms, which arise from mutual orthogonality of the LMOs. The delocalization of the π orbitals may seem small; however, as shown in Figure 1, isolated C═O and C═C chromophores in a bicyclic structure similar to norbornenone exhibit molar rotations well below 100 deg cm^2/dmol in magnitude (and which are not nearly as sensitive to the functional as for norbornenone[31]) whereas that of norbornenone is an order of magnitude larger and very strongly functional-dependent.

4.3. Optical Rotation Tensor Analysis. Figure 4 displays polar plots of the chiroptical response tensor ($\tilde{\mathbb{B}}$) calculated with different functionals at the Na D-line. The color and extension of the surfaces indicate the sign and magnitude of the principal components and the orientation of the PAS. The orientations of the PASs relative to the molecular frame are consistent among the calculations. The ordering of the principal components adopted here is 11 < 22 < 33 for $\tilde{\mathbb{B}}$. The components of $\boldsymbol{\beta}$ are given for the PAS of $\tilde{\mathbb{B}}$ and may not necessarily follow the same ordering. Numerical data for the tensor components are provided in Table 3. The strong increase of the magnitudes of both negative components in the

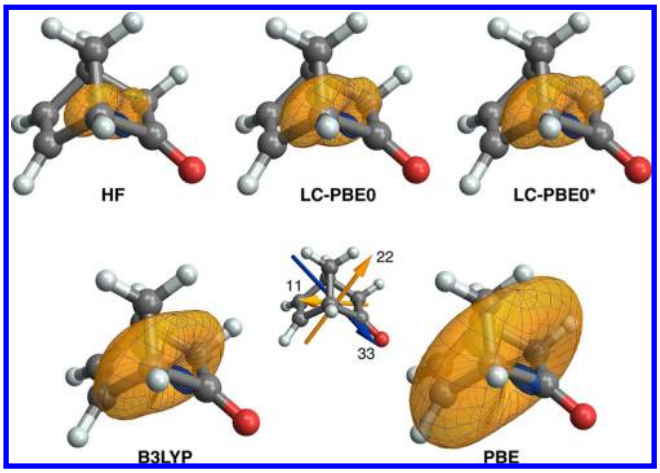

Figure 4. Polar plots of the chiroptical response tensor ($\tilde{\mathbb{B}}$) for norbornenone calculated with HF and different XC functionals at 589.3 nm. Yellow and blue indicate negative and positive optical rotation for a given direction. Surfaces were scaled to 25 pm per atomic unit. The principal axis system for LC-PBE0* is shown in the center. The origin is located at the CNC.

chiroptical response tensor from HF to PBE is readily apparent. In the adopted coordinate system, the most pronounced trend is found for the β_{33} component that spans a range of almost 12 au at 589.3 nm for the different functionals. By virtue of how the chiroptical response tensor is constructed (see SI), β_{33} enters both the 11 and the 22 component of $\tilde{\mathbb{B}}$. From the data, it therefore becomes apparent that the observed increase of components 11 and 22 of $\tilde{\mathbb{B}}$ (both are negative, Figure 4) upon varying the functional is driven almost entirely by the trend in β_{33}.

Since the OR depends on the frequency of the light wave, the static limit of $\boldsymbol{\beta}$ and the other tensors are also of interest (see Figure S3 in the SI for the corresponding $\tilde{\mathbb{B}}$ plots). The data in Table 3 demonstrates that a strong functional-dependence is already present at the static limit and becomes merely amplified as ω gets closer to an excitation frequency. Likewise, the fact that norbornenone has a large isotropic optical rotation is reflected in the large magnitude of the static $\boldsymbol{\beta}$, and the large difference between the tensor components, driven in particular by the large magnitude of β_{33}. We return to the balance between the different components in Section 4.4.

The fact that the variations of the OR for different functionals can be traced back to variations in β_{33}, and the fact that these variations are already present in the static limit, is very helpful. It allows us to focus on a single component of the tensor $\boldsymbol{\beta}$ in order to study the sensitivity of the norbornenone OR to electron delocalization and to uncover the origin of its magnitude. The PAS of $\tilde{\mathbb{B}}$ in Figure 4 (see also Figure S4)

Table 3. Diagonal Components of the Optical Tensors β and $\tilde{\mathbb{B}}$, in au, Calculated at the Static Limit and Sodium D-line in the Coordinate System Where the Chiroptical Response Tensor $\tilde{\mathbb{B}}$ is Diagonal[a]

ω (au)/λ (nm)	0/∞				0.07732/589.3			
component	11	22	33	iso	11	22	33	iso
β								
HF	10.73	−0.0637	−14.46	−1.266	11.95	−0.0344	−16.93	−1.670
LC-PBE0	9.875	0.4111	−15.18	−1.631	10.96	0.6124	−18.50	−2.310
LC-PBE0*	9.837	0.4526	−15.35	−1.687	10.91	0.6745	−18.73	−2.381
B3LYP	9.802	1.045	−17.44	−2.198	10.80	1.680	−22.50	−3.340
PBE	9.826	1.647	−20.42	−2.982	10.74	3.006	−28.74	−4.999
$\tilde{\mathbb{B}}$								
HF	−4.818	−1.802	2.820	−1.266	−5.827	−2.398	3.214	−1.670
LC-PBE0	−5.393	−2.585	3.086	−1.631	−6.840	−3.663	3.572	−2.310
LC-PBE0*	−5.483	−2.700	3.122	−1.687	−6.949	−3.814	3.619	−2.381
B3LYP	−6.348	−3.753	3.506	−2.198	−8.520	−5.706	4.207	−3.340
PBE	−7.764	−5.216	4.035	−2.982	−11.35	−8.752	5.106	−4.999

[a]'iso' indicates the isotropic values.

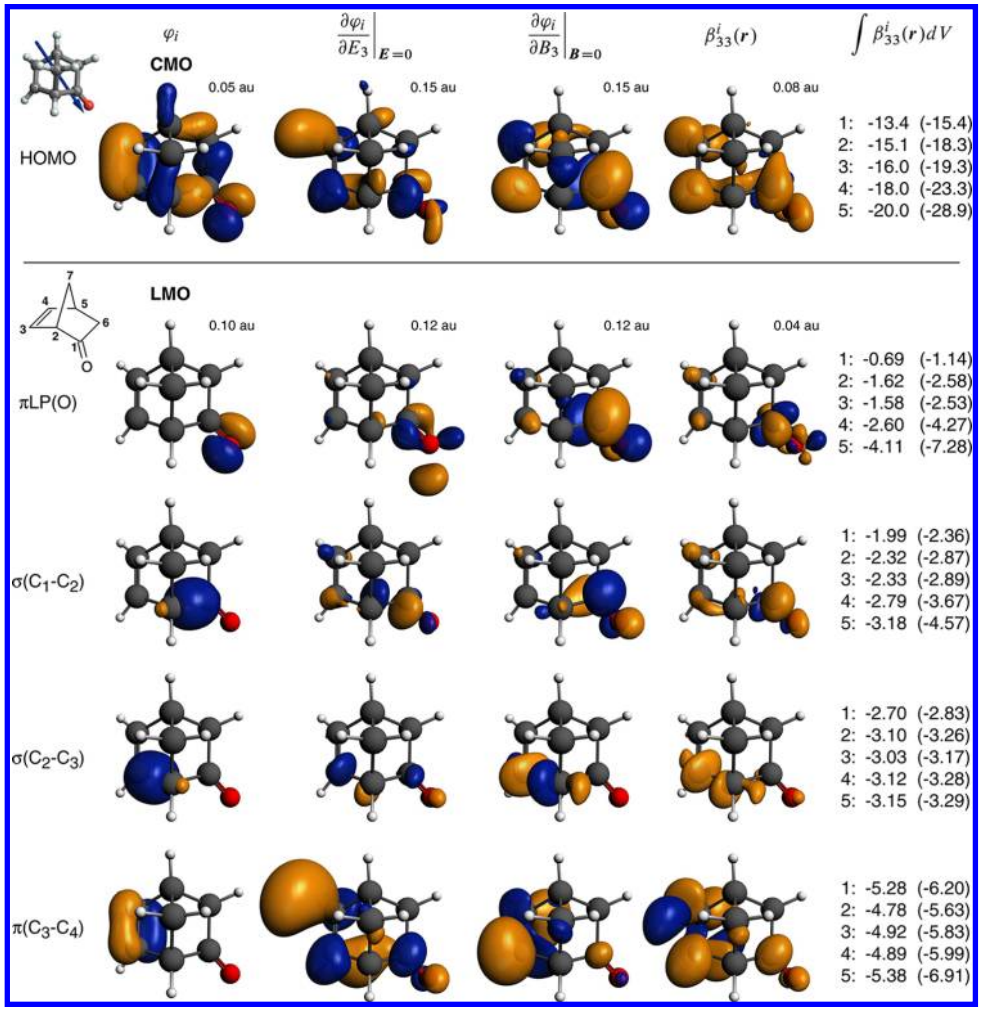

Figure 5. Dominant orbital contributions to β_{33} at the static limit. Numerical values for HF (1), LC-PBE0 (2), LC-PBE0* (3), B3LYP (4), and PBE (5) for $\lambda = \infty$ (in parentheses: 589.3 nm). Graphics from LC-PBE0* calculations, isosurface values in au as indicated. LP = lone pair.

shows that component 33 and the electric and magnetic fields used to calculate β_{33} are roughly parallel to the C═O bond and diagonal to the C═C bond.

Figure 5 displays selected dominant contributions from individual localized molecular orbitals (LMOs) and the canonical HOMO to β_{33}, as determined from eq 1, for different functionals, at the static limit (data for 589.3 nm are also provided). The full set of data for all significant orbitals can be found in the SI. Graphical representations of the orbitals, their electric-field and magnetic-field perturbations for the fields oriented along the 33 direction, and the product of the perturbations, are also shown in Figure 5 and in the SI. The

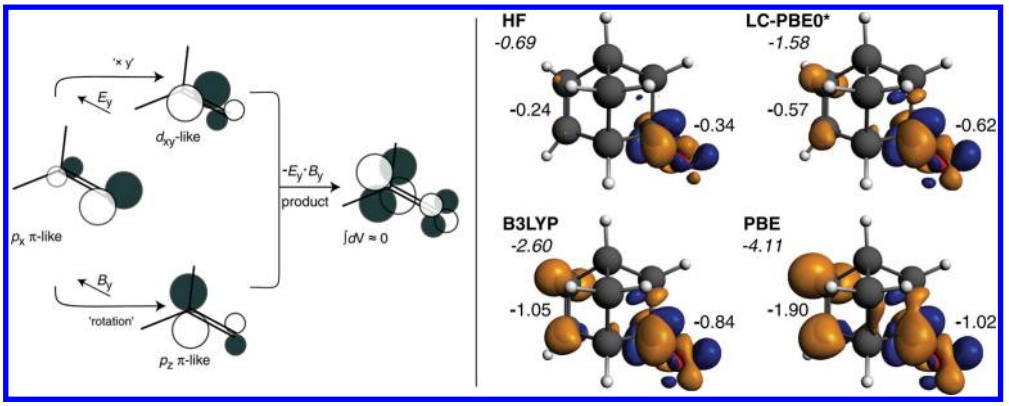

Figure 6. Left: Qualitative interpretation of the electric- and magnetic-field perturbations of the πLP(O) orbital at the carbonyl group via construction of the integrand of eq 1. Right: Static $\beta^i_{33}(\boldsymbol{r})$ for i = πLP(O) (isosurfaces 0.028 au). The numbers listed are the total orbital contributions to β_{33} obtained upon volume integration (italic), and approximate numerical integrations within low-value isosurfaces centered at the C═C and C═O moieties, respectively.

optical rotation component density $\beta^i_{33}(\boldsymbol{r})$ for orbital i represents the integrand in eq 1 for calculating β_{33}. In the usual delocalized CMO representation, the sensitivity to the choice of functional (i.e. the sensivity to the extent of electron delocalization) is almost entirely contained in the contribution from the HOMO. The HOMO also dominates β_{33}. The sum of contributions from all significant CMOs is very similar to that of the HOMO itself and to the total β_{33} (see Table S7, SI).

The HOMO is seen to be composed of AOs centered at the C═O and the C═C moiety as well as on the carbons bridging the chromophores. An interpretation of β_{33} in terms of individual bonds is not straightforward from the CMO analysis. However, the dominant HOMO contribution is certainly consistent with the dominance of the first excitation (HOMO to LUMO) in the SOS (Figure 1). Further, the HOMO indicates a role of the bridging carbons which may facilitate an electronic coupling between the two chromophores.

The localized MO (LMO) representation yields a number of orbitals with large contributions, as expected (Figure 5; see also the SI). Regarding the functional sensitivity, although all LMO contributions show variations with the functional to some degree, the oxygen π lone pair (LP) emerges as particularly important. In the PBE calculation, this orbital and the π orbital of the C═C bond are the largest negative individual contributors to β_{33}. Further, there are important contributions to β_{33} from the two σ bonds that connect the two chromophores. Of these two, the one adjacent to the carbonyl group also exhibits a pronounced sensitivity to the functional. For functionals other than PBE the largest contributors to β_{33} are π(C═C) and the σ orbitals of the bridge between C═C and C═O, while πLP(O) is of decreasing importance with increased HF exchange contribution. The data provide strong indications that the delocalization of one of the carbonyl oxygen lone pairs into the bicyclic system and delocalization of other bonds, which is physical but only to some extent, takes center stage when it comes to the performance of different electronic structure methods.

The LMO analysis shows that the σ bonds between carbon atoms 1, 2, and 3, facilitate the electronic coupling between the two chromophores. Consider, for instance, the products of the electric-field with the magnetic-field perturbed orbitals, which give the OR density functions $\beta^i_{33}(\boldsymbol{r})$. Per eq 1, the volume integral over $\beta^i_{33}(\boldsymbol{r})$ gives the contribution from a given LMO to the OR tensor component 33. Regions where these functions show sign changes will typically contribute less than regions where the sign is uniform. In the perturbed orbitals as well as in β^i_{33} one can clearly see magnitudes at distant centers that are related to the coupling between the chromophores. For instance, $\beta^i_{33}(\boldsymbol{r})$ for i = $\sigma(C_1{-}C_2)$ has a large magnitude at both chromophores. Likewise, $\beta^i_{33}(\boldsymbol{r})$ for i = $\sigma(C_2{-}C_3)$ shows a noticeable magnitude around the C═O moiety. As it has been discussed, some (unperturbed) LMOs have magnitudes at distant atoms that far exceed those expected from an orthogonality tail of a well-localized orbital (see Table 2 and Table S5 and Figure S2 (SI)). Therefore, the magnitudes of the bridging σ-orbital perturbations at the C═C and C═O groups must be associated with delocalization and electronic coupling between the chromophores. Likewise, πLP(O) and $\pi(C_3{-}C_4)$ show evidence for this type of coupling. In both cases, the $\beta^i_{33}(\boldsymbol{r})$ functions exhibit large magnitudes at the respective other chromophore and with uniform signs. Because of the uniform signs, these contributions do not vanish upon integration.

The particular sensitivity of the πLP(O) contribution to the extent of delocalization may be rationalized by considering how the electric-field and magnetic-field perturbed orbitals are expected to look like for a nonchiral isolated carbonyl chromophore with local C_{2v} symmetry, such as formaldehyde or acetone. A qualitative view is provided in Figure 6. Consider the oxygen π LP oriented along x, and the fields acting in y direction (along C═O). The action of the quantum mechanical operator for the electric field on the oxygen LP amounts to a multiplication of p_x with y, which yields approximately the shape of a d_{xy} orbital in the chromophore plane. The orbital field-derivative is composed of functions with similar local nodal patterns. The action of the magnetic field produces a rotation of the LP by 90 degrees around the field direction, giving the perturbed orbital roughly the shape of a carbonyl π^* orbital perpendicular to the LP (imaginary units in the operator not considered). Similar 'orbital rotation' models have long been used to rationalize trends in NMR chemical shifts through the action of the static magnetic field on the orbitals,[71,72] which we have summarized on our web page.[73] From the model in Figure 6, one would expect positive and negative terms in the integrand $\beta^i_{33}(\boldsymbol{r})$, around C═O, to cancel effectively upon integration as long as there is sufficiently high local symmetry. In norbornenone the local symmetry is lower due to the chirality of the molecule, but the sign pattern of the qualitative scheme in Figure 6 is indeed visible in the

juxtaposed $\beta^i_{33}(r)$ isosurface plots. The static perturbation (static limit of β) is easier to interpret in such a qualitative sense than the dynamic perturbation (the corresponding plots are shown in the SI, Figures S8 and S12), but in both cases, we observe comparable patterns in the orbital perturbations.

In the LMO plots for the πLP(O) orbital, it also becomes apparent that the region around the C═C moiety provides an important negative contribution where little to no cancellation of opposing signs occurs. A comparison for different functionals is shown next to the qualitative scheme in Figure 6. The magnitude of $\beta^i_{33}(r)$ around the C═C moiety for $i = \pi$LP(O) is particularly large for the nonhybrid PBE functional. It is small in HF theory where there is too little delocalization. The $\beta^i_{33}(r)$ around the carbonyl group appear similar for the different functionals but have different magnitudes. Because of the alternating sign patterns, integration around C═O gives relatively modest contributions to β_{33}. We have determined approximate contributions from the two functional groups by using numerical integration on a grid of points inside isosurfaces centered around C═O and C═C, respectively, which are generated with appropriately small isosurface values. The total numerical volume integrations agree well with the total values listed in Figure 6, which were obtained by analytical integration. Even for HF, the partial contribution from the C═C moiety in the C═O oxygen lone pair is significant (Figure 6). When going from HF to PBE, its magnitude rises much faster than the integral around the carbonyl group. The trends found for the delocalization contribution to β_{33} from πLP(O) around the C═C moiety are entirely consistent with the extent of the DFT delocalization error discussed in Section 4.2 and with the numerical data for the LMO delocalization in Table 2.

4.4. Large Magnitude of the Isotropic Optical Rotation of Norbornenone and Comparison with α-Pinene. We are finally in a position to address the question why the isotropic OR of norbornenone is so large, compared to structurally similar molecules with a single chromophore (C═C or C═O). For comparison, calculations were performed for α-pinene in its (*S*, *S*) absolute configuration (Figure 1). The computed Na D-line molar rotations of −63.51 (B3LYP), −81.93 (LC-PBE0),[31] and −79.5 (LC-PBE0*) (this work) agree reasonably well with coupled-cluster results (CCSD/aug-cc-pVDZ(C)+cc-pVDZ(H): −73.2 (MVG), −60.1 (LG)[28]) and the solution-phase experimental data (−70.3 deg cm^2/dmol).[23] The chiroptical response tensors of norbornenone and α-pinene calculated with LC-PBE0* are compared in Figure 7. For brevity, only the static limit is discussed. The PASs of the two tensors have similar orientations relative to the bicyclic cage and the C═C axis. Moreover, the tensor elements of α-pinene reach the same magnitude as those of norbornenone. The main difference in the isotropic optical activity of the two molecules is that in α-pinene two large tensor components (11 and 33) almost completely cancel in the isotropic average, whereas in norbornenone the cancellation is far less effective. This behavior can be traced back to the elements 11 and 33 of the OR tensor β. There is a sign change of the components relative to those of $\tilde{\mathbb{B}}$: β_{22} is small. β_{33} (negative) contributes to $\tilde{B}_{11}$ and $\tilde{B}_{22}$, and β_{11} (positive) contributes to $\tilde{B}_{22}$ and $\tilde{B}_{33}$. For α-pinene the roughly equal but opposite β_{11} and β_{33} cause the nearly vanishing $\tilde{B}_{22}$ and the nearly equal but opposite $\tilde{B}_{11}$ and $\tilde{B}_{33}$. In norbornenone, β_{22} is very small. The sizable negative $\tilde{B}_{22}$ and the large isotropic OR are both a result of $|\beta_{33}|$ being significantly larger than β_{11}.

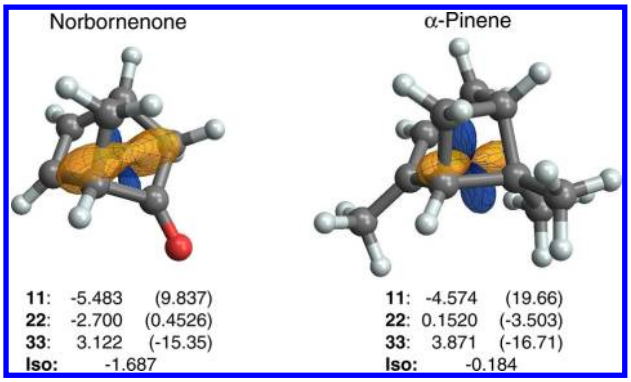

Figure 7. Static chiroptical response tensor $\tilde{\mathbb{B}}$ for norbornenone and α-pinene, and principal components, in au. Yellow and blue indicate negative and positive optical rotation for a given direction. Surfaces were scaled to 30 pm per atomic unit. LC-PBE0* functional. Values in parentheses are diagonal components of β.

Selected LMO data for the components of β are provided in Figure 8 (for full data set see the SI, Table S9). One of the large OR contributions in α-pinene comes from the π(C═C) orbital. The imbalance of positive and negative components for norbornenone and the near-perfect cancellation for α-pinene are clearly reflected in the π-bond contributions to the β-tensor elements. However, in terms of individual tensor elements, the C═C double bond emerges as strongly optically active for both norbornenone and α-pinene. Moreover, the plots of the densities $\beta^i_{11}(r)$ for π(C═C) appear very similar in both molecules. When considering that much of the magnitude of $\beta^i_{33}(r)$ for norbornenone is centered on the carbonyl group (more on this below), the optical activity of the C═C moiety in α pinene is even stronger than that in norbornenone. We tentatively attribute this finding to the twist angle of the double bond, that is, the C_2—C_3═C_4—C_5 dihedral angle. It adopts a value of 1° in norbornenone and 2° in α-pinene. For comparison, ethylene twisted in the same direction by 2° has an isotropic static β of −0.14, which is close to the −0.16 isotropic average for π(C═C) in α-pinene.

One of the major features for the π(C═C) contribution in norbornenone is seen to be the large negative 'tail' of $\beta^i_{33}(r)$ around C═O. Integration gives approximately −1 au in addition to the −3.5 au obtained from the integration around the C═C bond. There is no such imbalance in α-pinene; the isosurfaces of $\beta^i_{11}(r)$ and $\beta^i_{33}(r)$ are similar in appearance but have opposite sign patterns. It is clear from the previous sections that the large magnitude of $\beta^i_{33}(r)$ for the C═C π bond around the carbonyl group comes from the delocalization of π(C═C). In addition, as we have shown, there are several other orbitals that also contribute with large negative magnitudes to β_{33}, most notably the oxygen carbonyl lone-pair and the σ bonds bridging the two chromophores. These reinforcing contributions create the large imbalance between β_{11} and β_{33}, which ultimately causes the isotropic OR of norbornenone to be so large. In contrast, the contributions to β_{iso} from other orbitals in α-pinene cancel almost completely.

Finally, it is worthwhile to reiterate the importance of the relative orientations of the C═C and C═O bonds.[74] Figure S14 in the SI shows what happens to the optical rotation of a H_2C═CH—CH_2—CHO fragment, initially adopting the same geometry as the system of coupled chromophores in norbornenone, as it rotates around the C_2–C_3 single bond. The geometry enforced by the bicyclic cage in norbornenone is

dx.doi.org/10.1021/ct300839y | J. Chem. Theory Comput. 2012, 8, 4336–4346

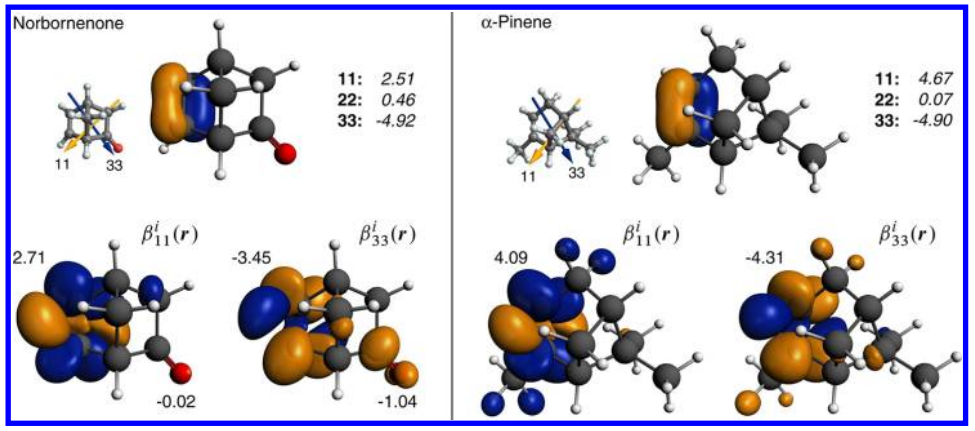

Figure 8. Top: Isosurfaces of the π(C═C) LMO (0.1 au), and their contributions to β tensor for norbornenone and α-pinene. Bottom: Isosurfaces (0.04 au) of $\beta^i_{11}(r)$ and $\beta^i_{33}(r)$ for π(C═C) and approximate numerical integrations within isosurfaces centered at the C═C and C═O moieties, respectively. LC-PBE0* functional.

seen to be nearly optimal for creating a large isotropic OR. In most other geometries, the cancellation of diagonal tensor elements is far more effective.

5. CONCLUSIONS

Electron delocalization plays a paramount role in the optical rotation (OR) of norbornenone. This conclusion is evident from an analysis in terms of individual 'chemist's orbitals' (localized MOs). Delocalization of the C═C π bond over the C═O group and delocalization of the carbonyl oxygen π lone-pair orbital over the C═C moiety result in a significantly enhanced component of the OR tensor in the direction of the C═O bond, β_{33}. Contributions from the bridging C−C σ bonds are also very important, as one might expect if delocalization between the C═C and C═O π orbitals is significant. The strong enhancement of the negative β_{33} is not balanced by other tensor components, which results in a large negative isotropic optical rotation of norbornenone. A comparison with α-pinene, which has a more localized C═C π bond as a composition of the corresponding 'natural LMO' revealed (magnitudes below <0.4% on adjacent and distant carbons, compare Table 2), clearly shows how geometry and electronic structure effects in norbornenone all cooperate to yield an enhancement of β_{33}.

In an interesting twist, deficiencies in commonly applied density functionals have provided important clues about the outstanding role of electron delocalization in causing the large OR of norbornenone. Different classes of approximate functionals on the one hand, and HF theory on the other hand, allow us to study what happens to the OR if there is too much or not enough delocalization. We have shown that an optimal-tuning procedure based on ab initio criteria can lead to a density functional that, presumably, gives the physically correct extent of C═C π bond and C═O oxygen π lone-pair delocalization in the system.

It is clear that one can dig much deeper in an attempt to fully rationalize the magnitudes and the signs of all orbital contributions to the optical activity of norbornenone, α-pinene, and countless other molecules. The present work is intended to provide an initial assessment of the analysis technique and to address long-standing problems with OR calculations for norbornenone. Further, we hope to have demonstrated that with suitable theoretical tools it is possible to gain an in-depth understanding of optical rotation. We expect to be able to provide additional examples in subsequent publications and, in particular, consider the optical rotation created by chiral σ-frameworks.

■ ASSOCIATED CONTENT

Supporting Information

Details of the OR analysis protocol. Comparison of the GIAO-length, AO-length, and MVG results of OR calculations. Details of two-dimensional tuning procedure. Chiroptical data for the tuned set of functionals. Additional graphical and numerical data for analysis of the OR of norbornenone and α-pinene. This material is available free of charge via the Internet at http://pubs.acs.org.

■ AUTHOR INFORMATION

Corresponding Author

*E-mail: jochena@buffalo.edu.

Notes

The authors declare no competing financial interest.

■ ACKNOWLEDGMENTS

This research has been supported by the National Science Foundation, Grant No. CHE 0952253 to J.A. M.S. is grateful for financial support from the Foundation for Polish Science (START scholarship) as well as from the Polish Ministry of Science and Higher Education (Mobility Plus program). We thank the Center for Computational Research at the University at Buffalo for supporting our research. We also thank Lucia Nitsch-Velasquez for calculating the data used to prepare Figure 1.

■ REFERENCES

(1) Tinoco, I., Jr *Adv. Chem. Phys.* **1962**, *4*, 113−160.
(2) Applequist, J. *Acc. Chem. Res.* **1977**, *10*, 79−85.
(3) Kirkwood, J. G. *J. Chem. Phys.* **1937**, *5*, 479−491.
(4) Moffitt, W. *J. Chem. Phys.* **1956**, *25*, 467−478.
(5) Bayley, P. M.; Nielsen, E. B.; Schellmann, J. A. *J. Phys. Chem.* **1969**, *73*, 228−243.
(6) Berova, N.; Di Bari, L.; Pescitelli, G. *Chem. Soc. Rev.* **2007**, *36*, 914−931.
(7) di Bari, L.; Pescitelli, G. Electronic circular dichroism. In *Computational Spectroscopy. Methods, Experiments, and Applications*; Grunenberg, J., Ed.; Wiley-VCH: Weinheim, 2010; pp 241−277.
(8) Tinoco, I. J.; Woody, R. W. *J. Chem. Phys.* **1964**, *40*, 160−165.

(9) Volosov, A.; Woody, R. W. Theoretical approach to natural electronic optical activity. In *Circular Dichroism. Principles and Applications*; Nakanishi, K., Berova, N., Woody, R. W., Eds.; VCH: New York, 1994; pp 59−84.
(10) Polavarapu, P. L. *Chem. Rec.* **2007**, *7*, 125−136.
(11) Autschbach, J. *Chirality* **2009**, *21*, E116−E152.
(12) Crawford, T. D. *Theor. Chem. Acc.* **2006**, *115*, 227−245.
(13) Pecul, M.; Ruud, K. The ab initio calculation of optical rotation and electronic circular dichroism. In *Advances in Quantum Chemistry*, Vol. *50*; Elsevier: San Diego, 2005; pp 185−212.
(14) Stephens, P. J.; McCann, D. M.; Cheeseman, J. R.; Frisch, M. J. *Chirality* **2005**, *17*, S52−S64.
(15) Mukhopadhyay, P.; Wipf, P.; Beratan, D. N. *Acc. Chem. Res.* **2009**, *42*, 809−819.
(16) Kondru, R. K.; Wipf, P.; Beratan, D. N. *Science* **1998**, *282*, 2247−2250.
(17) Kondru, R. K.; Wipf, P.; Beratan, D. N. *J. Am. Chem. Soc.* **1998**, *120*, 2204−2205.
(18) Murphy, V. L.; Kahr, B. *J. Am. Chem. Soc.* **2011**, *133*, 12918−12921.
(19) Claborn, K.; Isborn, C.; Kaminsky, W.; Kahr, B. *Angew. Chem., Int. Ed.* **2008**, *47*, 5706−5717.
(20) Moscowitz, A. *Adv. Chem. Phys.* **1962**, *4*, 67−112.
(21) Lightner, D. A.; Gawronski, J. K.; Bouman, T. D. *J. Am. Chem. Soc.* **1980**, *102*, 5749−5754.
(22) Plettner, E.; Mohle, A.; Mwangi, M. T.; Griscti, J.; Patrick, B. O.; Nair, R.; Batchelor, R. J.; Einstein, F. *Tetrahedron: Asymmetry* **2005**, *16*, 2754−2763.
(23) Johnson, W. S.; Frei, B.; Gopalan, A. S. *J. Org. Chem.* **1981**, *46*, 1512−1513.
(24) Stephens, P. J.; Devlin, F. J.; Cheeseman, J. R.; Frisch, M. J. *J. Phys. Chem. A* **2001**, *105*, 5356−5371.
(25) Wiberg, K. B.; Wang, Y. G.; Wilson, S. M.; Vaccaro, P. H.; Cheeseman, J. R. *J. Phys. Chem. A* **2006**, *110*, 13995−14002.
(26) Ruud, K.; Stephens, P. J.; Devlin, F. J.; Taylor, P. R.; Cheeseman, J. R.; Frisch, M. J. *Chem. Phys. Lett.* **2003**, *373*, 606−614.
(27) Crawford, T. D.; Tam, M. C.; Abrams, M. L. *J. Phys. Chem. A* **2007**, *111*, 12057−68.
(28) Crawford, T. D.; Stephens, P. J. *J. Phys. Chem. A* **2008**, *112*, 1339−1345.
(29) Mach, T. J.; Crawford, T. D. *J. Phys. Chem. A* **2011**, *115*, 10045−10051.
(30) Srebro, M.; Autschbach, J. *J. Chem. Theory Comput.* **2012**, *8*, 245−256.
(31) Srebro, M.; Govind, N.; de Jong, W.; Autschbach, J. *J. Phys. Chem. A* **2011**, *115*, 10930−10949.
(32) Kundrat, M. D.; Autschbach, J. *J. Am. Chem. Soc.* **2008**, *130*, 4404−4414.
(33) Nitsch-Velasquez, L.; Autschbach, J. *Chirality* **2010**, *22*, E81−E95.
(34) Autschbach, J.; Nitsch-Velasquez, L.; Rudolph, M. *Top. Curr. Chem.* **2011**, *298*, 1−98.
(35) Krykunov, M.; Kundrat, M. D.; Autschbach, J. *J. Chem. Phys.* **2006**, *125*, 194110.
(36) Autschbach, J. *ChemPhysChem* **2011**, *12*, 3224−3235.
(37) Autschbach, J. Ab initio ECD and ORD—From organic molecules to transition metal complexes. In *Advances in Chiroptical Methods*; Berova, N., Polavarapu, P., Nakanishi, K., Woody, R., Eds.; Wiley Blackwell: New York, 2011; pp 593−642.
(38) Buckingham, A. D.; Dunn, M. B. *J. Chem. Soc. A* **1971**, 1988−1991.
(39) Graham, E. B.; Raab, R. E. *Proc. R. Soc. Lond. A* **1990**, *430*, 593−614.
(40) Amos, R. D. *Chem. Phys. Lett.* **1982**, *87*, 23−27.
(41) Bylaska, E. J. et al. *NWChem, A Computational Chemistry Package for Parallel Computers*, Version 6.1 (2012 developer's version); Pacific Northwest National Laboratory: Richland, WA, 2012.
(42) Valiev, M.; Bylaska, E. J.; Govind, N.; Kowalski, K.; Straatsma, T. P.; Van Dam, H. J. J.; Wang, D.; Nieplocha, J.; Apra, E.; Windus, T. L.; de Jong, W. A. *Comput. Phys. Commun.* **2010**, *181*, 1477−1489.
(43) Perdew, J. P.; Burke, K.; Ernzerhof, M. *Phys. Rev. Lett.* **1998**, *80*, 891.
(44) Adamo, C.; Barone, V. *J. Chem. Phys.* **1999**, *110*, 6158−6170.
(45) Ernzerhof, M.; Scuseria, G. E. *J. Chem. Phys.* **1999**, *110*, 5029−5036.
(46) Srebro, M.; Autschbach, J. *J. Phys. Chem. Lett.* **2012**, *3*, 576−581.
(47) Weigend, F.; Ahlrichs, R. *Phys. Chem. Chem. Phys.* **2005**, *7*, 3297−3305.
(48) Ahlrichs, R.; et al. *Turbomole, Version 5.7*; Quantum Chemistry Group, Universitat Karlsruhe: Karlsruhe, Germany, 2004.
(49) Dunning, T. H., Jr. *J. Chem. Phys.* **1989**, *90*, 1007−1023.
(50) Kendall, R. A.; Dunning, T. H.; Harrison, R. J. *J. Chem. Phys.* **1992**, *96*, 6796.
(51) Krykunov, M.; Autschbach, J. *J. Chem. Phys.* **2005**, *123*, 114103−10.
(52) Pedersen, T. B.; Koch, H.; Boman, L.; Sánchez de Merás, A. M. J. *Chem. Phys. Lett.* **2004**, *393*, 319−326.
(53) Becke, A. D. *J. Chem. Phys.* **1993**, *98*, 5648−5652.
(54) Lee, C.; Yang, W.; Parr, R. G. *Phys. Rev. B* **1988**, *37*, 785−789.
(55) Stephens, P. J.; Chabalowski, C. F.; Devlin, F. J.; Jalkanen, K. J. *Chem. Phys. Lett.* **1994**, *225*, 247−257.
(56) Rohrdanz, M. A.; Herbert, J. M. *J. Chem. Phys.* **2008**, *129*, 034107.
(57) Pipek, J.; Mezey, P. G. *J. Chem. Phys.* **1989**, *90*, 4916−4926.
(58) Glendening, E. D.; Badenhoop, J. K.; Reed, A. E.; Carpenter, J. E.; Bohmann, J. A.; Morales, C. M.; Weinhold, F. *NBO 5.0*; Theoretical Chemistry Institute, University of Wisconsin: Madison, WI, 2001; http://www.chem.wisc.edu/~nbo5 (accessed Sept. 2012).
(59) Autschbach, J.; Ziegler, T.; Patchkovskii, S.; van Gisbergen, S. J. A.; Baerends, E. J. *J. Chem. Phys.* **2002**, *117*, 581−592.
(60) Lightner, D. A.; Beavers, W. A. *J. Am. Chem. Soc.* **1971**, *93*, 2677−2684.
(61) Cohen, A. J.; Mori-Sánchez, P.; Yang, W. *Science* **2008**, *321*, 792−794.
(62) Mori-Sánchez, P.; Cohen, A. J.; Yang, W. *Phys. Rev. Lett.* **2008**, *100*, 146401.
(63) Kuritz, N.; Stein, T.; Baer, R.; Kronik, L. *J. Chem. Theory Comput.* **2011**, *7*, 2408−2415.
(64) Levy, M.; Perdew, J. P.; Sahni, V. *Phys. Rev. A* **1984**, *30*, 2745−2748.
(65) Baer, R.; Livshits, E.; Salzner, U. *Annu. Rev. Phys. Chem.* **2010**, *61*, 85−109.
(66) Kronik, L.; Stein, T.; Refaely-Abramson, S.; Baer, R. *J. Chem. Theory Comput.* **2012**, *8*, 1515−1531.
(67) Stein, T.; Kronik, L.; Baer, R. *J. Chem. Phys.* **2009**, *131*, 244119 (5 pages).
(68) Autschbach, J. *ChemPhysChem* **2009**, *10*, 1−5.
(69) Autschbach, J. *J. Chem. Educ.* **2012**, *89*, 1032−1040.
(70) Weinhold, F. Natural bond orbital methods. In *Encyclopedia of Computational Chemistry*; von Ragué Schleyer, P., Ed.; John Wiley & Sons: Chichester, 1998; pp 1792−1811.
(71) Grutzner, J. B. Chemical shift theory. Orbital symmetry and charge effects on chemical shifts. In *Recent Advances in Organic NMR Spectroscopy*; Norell Press: Landisville, NJ, 1987; pp 17−42.
(72) Autschbach, J.; Zheng, S. *Magn. Reson. Chem.* **2008**, *46*, S48−S55.
(73) http://ja01.chem.buffalo.edu/~jochena/research/orbitalrotations.html (accessed Sept. 2012).
(74) Wiberg, K. B.; Vaccaro, P. H.; Cheeseman, J. R. *J. Am. Chem. Soc.* **2003**, *125*, 1888−1896.
(75) Vaccaro, P., Yale University, private communication, 2012.
(76) Moore, B., II; Autschbach, J. *ChemistryOpen* **2012**, *1*, 184−194.